Amphiphilic phosphorus dendrons-associated with anti-inflammatory siRNA reduce symptoms in murine collagen-induced arthritis

Zhibo Yu, Nicolas Tsapis, François Fay, Liang Chen, Andrii Karpus, Xiangyang Shi, Catherine Cailleau, Samuel García Pérez, Nicolas Huang, Juliette Vergnaud, et al.

Amphiphilic phosphorus dendrons-associated with anti-inflammatory siRNA reduce symptoms in murine collagen-induced arthritis

Zhibo Yu[1], Nicolas Tsapis[1], François Fay[1], Liang Chen[2,3], Andrii Karpus[2 3], Xiangyang Shi[4], Catherine Cailleau[1], Samuel García Pérez[5], Nicolas Huang[1], Juliette Vergnaud[1], Serge Mignani[6,7], Jean-Pierre Majoral[2], Elias Fattal[1*]

[1] Université Paris-Saclay, CNRS, Institut Galien Paris-Saclay, 91400 Orsay, France,
[2]Laboratoire de Chimie de Coordination, CNRS, Université de Toulouse 31077 Toulouse Cedex 4, France
[3]Université Toulouse 118 route de Narbonne 31077, Toulouse Cedex4, France
[4]College of Chemistry, Chemical Engineering and Biotechnology, Donghua University, Shanghai, 201620, PR China
[5]Rheumatology & Immuno-mediated Diseases Research Group (IRIDIS), Galicia Sur Health Research Institute (IIS Galicia Sur), Sergas-Uvigo, Spain
[6]University Paris Descartes, Pres Sorbonne Paris Cité, CNRS UMR 860, Laboratoire de Chimie et Biochimie Pharmacologiques et Toxicologique, 45 rue des Saints Peres,75006, Paris, France
[7]CQM - Centro de Química da Madeira, Universidade da Madeira, Funchal 9020-105, Portugal

ABSTRACT

Small interfering RNA (siRNA) holds promise for treating rheumatoid arthritis by inhibiting major cytokines such as TNF-α. We developed original cationic amphiphilic phosphorus dendrons to produce dendriplexes associated with an anti-tumor necrosis factor-α (TNF-α) siRNA. The dendrons were made of 10 pyrolidinium end groups and a C17 aliphatic chain. The dendriplexes demonstrated the ability to protect siRNA from nuclease degradation and to promote macrophage uptake. Moreover, they led to potent inhibition of TNF-α expression in the lipopolysaccharide-activated mouse macrophage cell line RAW264.7 *in vitro* model. A significant anti-inflammatory effect in the murine collagen-induced arthritis model was observed through arthritis scoring and histological observations. These results open up essential perspectives in using this original amphiphilic dendron to reduce the disease burden and improve outcomes in chronic inflammatory disease.

KEYWORDS: amphiphilic dendron; micelles; delivery system; TNF-α; siRNA; rheumatoid arthritis.

INTRODUCTION

RNA interference employing small interfering RNA (siRNA) is a potent alternative to antibodies as it can specifically silence one target gene and block protein expression[1]. In several diseases, various siRNAs delivered by galactosylated conjugates or lipid nanoparticles targeting liver cells have recently been approved[2,3]. The newly FDA-approved lipid nanoparticles Patisiran (branded Onpattro®) knocks down a mutated form of the transthyretin gene that produces a dysfunctional protein causing myeloid deposits in the nervous system tissue, the heart, and other organs[4]. These recent successes are related to the ability of the designed carrier to protect siRNA against degradation and deliver it intact to hepatocytes, the liver being a target for lipid nanoparticles[5]. Although liver targeting of siRNA is a significant achievement, allowing siRNA to reach other tissues remains a critical issue that our group and others strive to solve by developing novel nanoparticulate platforms.

This study focuses on the delivery of an anti-tumor necrosis factor-α (TNF-α) siRNA to treat rheumatoid arthritis (RA)[6,7]. RA is an autoimmune and systemic inflammatory disorder that affects 0.5 to 1.1% of developed countries' population[8]. RA is characterized by synovitis, cellular infiltration, particularly immune cells, and intense inflammation flares that evolve into bone erosion and cartilage destruction[9]. These severe symptoms may lead to disability and systemic complications, resulting in a severe decrease in the patient's quality of life and a reduction in life expectancy[10]. Pro-inflammatory cytokines, including TNF-α, interleukin-1, and interleukin-6, play a crucial role in the progression of RA and have been widely described as targets[11]. Among these cytokines, TNF-α is highly prominent as it induces the release of other cytokines in the RA synovium, causing chronic inflammation[12]. Anti-TNF-α antibodies such as infliximab, adalimumab, and golimumab, as well as TNF inhibitors such as etanercept have been widely clinically used as they block the effect of TNF-α[13]. However, repeated administration of biologics induces side effects and triggers opportunistic infections[14], and additional clinical studies have estimated that about half of the patients interrupt the treatment due to side effects[15]. Delivery of anti-TNFα siRNA using nanocarriers is a potent strategy due to their accumulation in the inflamed region thanks to their extravasation through leaky vasculature and subsequent inflammatory cell-mediated sequestration (ELVIS)[16,17]. Most

of the studies using nanocarriers were carried out with micelles or nanoparticles. Micelles are unique self-assembled nanostructures. In cationic micelles, the hydrophilic shell with positive charges enables the complexation of the negatively charged siRNA by electrostatic interaction and its protection against nuclease degradation[18]. Micelles have also been shown to be able to bind and cross the cell membrane, which facilitates and enhances siRNA delivery to the cell cytosol and further gene inhibition[19]. siRNA molecules have been successfully associated with various micelles or nanoparticles displaying polyethyleneimine end groups, although this type of functional group has been demonstrated to be toxic[20].

In previous work, we have shown that dendrimers of the 3rd generation, bearing pyrrolidinium groups, can deliver an anti-TNF-α siRNA through the pulmonary route in a murine acute lung injury model [21,22]. These dendrimers are highly biocompatible, do not display any toxicity, and are equivalent to PAMAM dendrimers in silencing the cascade of cytokine expression[21,22].

This study investigates an alternative strategy consisting of cationic amphiphilic dendrimers called dendrons [23]. We assessed the ability of new cationic phosphorus dendrons to form micelles and deliver siRNA *in vitro* and *in vivo*. The dendron made of 10 pyrolidinium end groups and a C17 aliphatic chain was able to efficiently complex anti-TNF-α siRNA and form dendriplexes. Those complexes showed an excellent cell binding affinity and allowed siRNA protection against enzymatic degradation. Subsequent *in vitro* and *in vivo* investigations demonstrated the ability of these dendriplexes to silence TNF-α in the LPS-activated macrophage model effectively and to lead to symptom reduction in a murine collagen-induced arthritis model. Therefore, we believe these dendriplexes should be considered an alternative approach to other amphiphilic carriers for siRNA delivery.

EXPERIMENTAL SECTION

Materials

All chemicals were purchased from Acros, Aldrich, or Fluka. All solvents were freshly dried and distilled according to routine procedures before use. Asymmetric duplex siRNA

directed against TNF-α, fluorescent dicer substrate siRNA labeled with FAM (fluorescein amidite), and the negative control sequence were purchased from Eurogentec (Eurogentec, Angers, France) as dried, purified, and desalted duplexes. The oligonucleotide sequences in the anti-TNF-α siRNA were the following:

sense 5'-GAC-AAC-CAA-CUA-GUG-GUG-cdtdt-3',

anti-sense 5'-GCA-CCA-CUA-GUU-GGU-UGU-cdtdt-3'.

A negative control siRNA with the same number of bases as anti-TNF-α siRNA was used. The exact sequence was not provided by the supplier (Eurogentec). Dulbecco's phosphate buffer saline, 3-(4,5-dimethylthiazol-2-Yl)-2,5-diphenyltetrazolium bromide (MTT), hydrogen chloride (HCl), sodium hydroxide (NaOH), and lipopolysaccharide from *Escherichia coli* O111:B4 (LPS) (γ-irradiated, < 1 % protein) were obtained from Sigma-Aldrich (St Quentin Fallavier, France). Lactate dehydrogenase (LDH) kit was acquired from Promega (Charbonnières-Les-Bains, France). RNase-free water (Sigma-Aldrich, St Quentin Fallavier, France) was used for all solutions containing siRNA and dendrimers. All additional chemicals used were of analytical grade.

Synthesis and characterization of amphiphilic dendrons

All handling were carried out using a standard dry argon-high vacuum technique. Organic solvents were dried and distilled before use. Dichloro thiophospho methylhydrazine was obtained as previously described[24] and used without further purification as a solution in $CHCl_3$. Dendrimer core AB_5 was synthesized according to previously published procedures[25]. Figure 1 summarizes the synthesis of the C17P10 dendron. AB_5 dendrimer with P-Cl_2 surface (0.264 mmol) and anhydrous magnesium sulfate (0.5 g, 4.15 mmol) were mixed in 20 mL THF. The solution was cooled to 0 °C. To this solution kept at 0 °C, DIPEA (3.9 mmol) was added, followed by the slow addition of alkyl diamine, then stirred for 4 to 6 h. After completion of the reaction controlled by ^{31}P NMR, the solvent was evaporated under vacuum, and the solid residue was extracted with dichloromethane (DCM) (100 mL) and 10% K_2CO_3 solution (w/v) in water (50 mL). The organic layer was dried over sodium sulfate and then evaporated under reduced pressure. The residue was dissolved in 10 mL of tetrahydrofuran (THF) and precipitated in 100 mL pentane. The resulting solution was stirred for 1 h and then filtered under argon to obtain a white

powder that was subsequently dried under vacuum. Terminal amino groups of the dendrons were further protonated using 1M hydrogen chloride solution in diethyl ether, leading to water-soluble amphiphilic dendrons.

^{1}H, $^{13}C\{^{1}H\}$, and $^{31}P\{^{1}H\}$ NMR spectra were recorded using AV300PAS, AV400PAS, AV400LIQ spectrometers (Bruker, Germany). To assign the ^{13}C NMR signals, Jmod, HMBC, and HBQC NMR experiments were carried out when necessary. Protonated dendrimers were characterized only by $^{31}P\{^{1}H\}$ NMR to ensure the integrity of the structures. Unfortunately, mass spectrometry could not be used to prove the purity of these dendrimers because of spontaneous rearrangements in the phosphorhydrazone structure during the analysis[26].

The chemical characterizations of dendron by NMR are the following:

^{1} H NMR (400 MHz, $CDCl_3$) δ = 7.51-7.43 (m, 15H), 7.03-6.85 (m, 12H), 6.68-6.66 (m, 2H), 6.36 (t, J = 8 Hz, 1H), 4.18-4.05 (m, 10H), 3.33-3.28 (m, 2H), 3.18-2.96 (m, 35H), 2.69-2.49 (m, 60H), 2.16 (t, J = 8Hz, 2H), 1.63-1.59 (m, 2H), 1.26 (s, 30H), 0.89 (t, J = 8Hz, 3H). (Yield = 71%).

^{31}P NMR (121 MHz, $CDCl_3$) δ = 68.37, 67.92, 8.57.

^{13}C NMR (100 MHz, $CDCl_3$)δ = 173.31, 150.72, 150.64, 135.81, 135.66, 132.90, 132.78, 129.46, 127.46, 127.40, 121.11, 120.66, 56.23, 56.14, 53.78, 40.85, 39.80, 36.74, 35.36, 30.76, 30.67, 30.64, 30.54, 29.70, 29.68, 29.65, 29.57, 29.46, 29.41, 29.35, 25.84, 23.54, 22.68, 14.12.

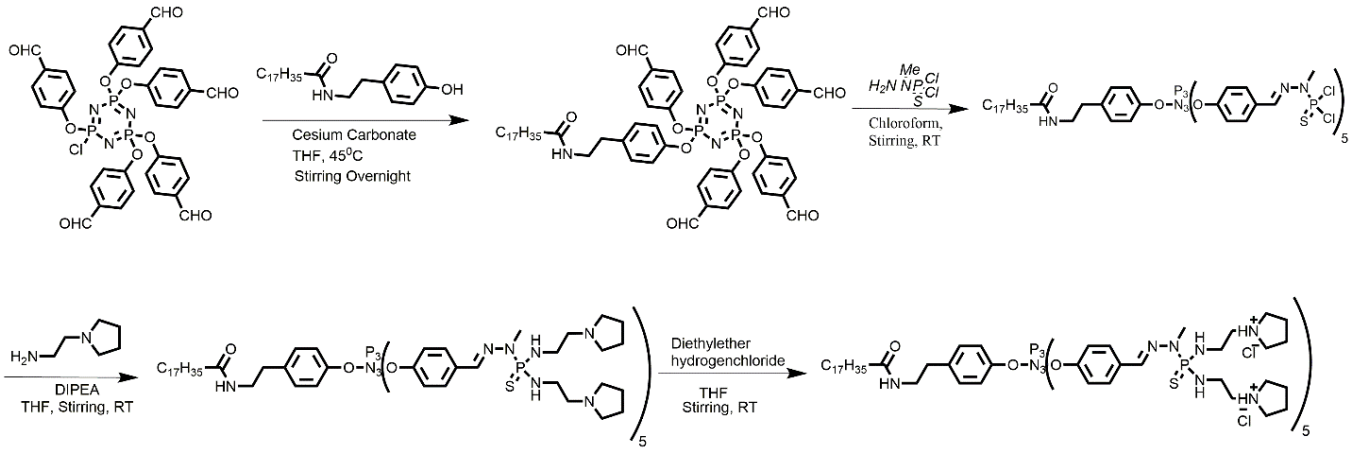

Figure 1. Synthesis of the C17P10 amphiphilic dendron: the upper part of synthesis has been described elsewhere and leads to the AB_5 core[25]. C17P10 amphiphilic dendron bears 10 pyrrolidinium end-groups and a C_{17} aliphatic chain.

Critical micelle concentration

Critical micelle concentration (CMC) is an essential characteristic of amphiphilic dendrons. It was determined by measuring surface tension as a function of dendron concentration (0.02 - 5mM in PBS) using the pendant drop method employing a tracker tensiometer (Teclis, Civrieux d'Azergues, France). Measurements were performed on 9 drops of 10 µL for each concentration. The shape of the drop was computed 60 seconds after its formation. Experimentally, the CMC was determined from the surface tension plot's inflection point versus the amphiphilic dendron concentration (semi-log plot). The equations describing the two linear parts of the plot were established using linear regression. The CMC was then obtained from the intersection of these two lines.

Preparation and characterization of C17P10 dendriplexes

3.2 mg of dendron were dissolved in 1 mL of PBS buffer to obtain a concentration of 1 mM. This solution was mixed with a specific volume of a 5 µM siRNA stock solution to prepare dendriplexes (called C17P10 dendriplexes) at N/P ratios (the molar charge ratio between the dendron and the anionic siRNA) of 5, 10, 15, and 20. Size distribution, polydispersity index (PdI), and zeta potential were measured using dynamic light scattering (DLS) (Zetasizer Nano ZS90 or Nanosizer Ultra, Malvern, UK) operating at a scattering angle of 173°. Dendron solutions and C17P10 dendriplexes were prepared in 1 mM PBS buffer at pH 7.4, and measurements were performed in triplicate at 25°C. The binding affinity of dendrons and siRNA at different N/P ratios were assessed by agarose gel electrophoresis. Gels were run at 120 V for 20 min in a Tris-borate-EDTA (TBE) buffer (pH 8.2) supplemented with 5 µL of 2.5 mg/mL ethidium bromide. The images of the gels were obtained using a BIO-RAD chemidoc MP Imaging System (Marnes-la-Coquette, France).

SiRNA complexation efficacy by C17P10 dendrons

The complexation efficacy of siRNA by amphiphilic dendrons was determined by fluorescent measurement using the QuantiFluor® dye (Promega, France) as a function of N/P ratio. Since dendrons quenched QuantiFluor® fluorescence, the complexation efficacy was determined indirectly by evaluating non-complexed siRNA. C17P10

dendriplexes at the N/P ratio of 5 and 10 were prepared as described above and were then centrifiltered (AMICON, Merck, MWCO = 15kDa) at 10, 000 g for 10 min. 500µL of 200-fold Quantifluor dye diluted in TE buffer was added to the filtered solution containing non-complexed siRNA and vortexed to ensure the binding between siRNA and dye. RNA standard samples with a concentration range between 31.25 and 2000 ng/mL were prepared and mixed with 200-fold Quantifluor dye diluted in TE buffer. A calibration curve was obtained using a spectrofluorometer (excitation 492nm, emission 540nm). The concentration of free siRNA in the solution was determined from this curve. The complexation efficacy of dendriplexes was calculated by the percentage of free siRNA to total siRNA.

Stability of siRNA in C17P10 dendriplexes against RNase degradation

The protection of siRNA in C17P10 dendriplexes against RNase degradation was assessed as follows.13 aliquots of 250 µL of C17P10 dendriplexes at an N/P ratio of 5 were prepared. These aliquots were then incubated at 37 °C in RNase solution at 0.01 µg/mL for different durations (0, 5, 10, 15, 20, 25, 30, 45, 60, 75, 90, 105 and 120 min). Aliquots (300 µL) of each solution were withdrawn, added to 100 µL of 1% SDS solution, and kept on ice. SDS was used to decomplex siRNA from C17P10 dendrons. The resulting solutions were analyzed using agarose gel electrophoresis and visualized using BIO-RAD chemidoc MP Imaging System (Bio-Rad, Marnes-la-Coquette, France). Non-complexed siRNA not incubated with RNase was used as a positive control, while non-complexed siRNA treated with RNase A was used as a negative control.

Transmission electron microscopy

Dendron solution and C17P10 dendriplexes with the corresponding dendron concentration of 0.8 mg/mL were prepared, respectively. 5.5 µL of these solutions were gently deposited on a standard carbon-coated copper transmission electron microscopy (TEM) grid and allowed to dry at room temperature. The grid was stained with osmium tetroxide steam (4% osmium tetroxide) for 1 minute. The samples were subsequently observed with a JEOL 1400 transmission electron microscope operating at 120 KV.

Cell culture

The mouse macrophage cell line Raw 264.7 was obtained from American Type Culture Collection (ATCC) and used between passages 3 and 20. Cells were maintained at 37 °C, 5% CO_2 in Dulbecco's Modified Eagle's Medium (DMEM) (Sigma-Aldrich, St. Louis, MO, USA) supplemented with 10% (v/v) fetal bovine serum (FBS) (PAA Laboratories, Pasching, Austria), 100 U/mL penicillin, and 100 μg/mL streptomycin.

MTT assay and lactate dehydrogenase release assay

Raw 264.7 cells were seeded at 8×10^3 cells/well in a 96-well plate and allowed to grow overnight. Dendriplexes were diluted in a fresh medium to obtain different concentrations. Cells were incubated with dendriplexes for 24 h. 20 µL of 3-(4,5-dimethylthiazol-2-yl)-2,5-diphenyltetrazolium bromide (MTT) (5 mg/mL) was added to each well and incubated for 4 h to transform it into formazan crystals. The medium was then removed, and the formazan crystals were dissolved by adding 200 µL of dimethyl sulfoxide (DMSO). The DMSO solution's optical density (OD) was read at 570 nm using a microplate reader (fluostar OPTIMA, BMG labtech, Champigny-sur-Marne, France). The viability of cells was calculated as a percentage by comparing the OD value of treated with non-treated cells. All samples were run in triplicate.

For lactate dehydrogenase (LDH) release assay, Raw 264.7 cells were treated with different concentrations (0 – 120 nM) of dendriplexes for 24h. A commercial LDH kit (cytotox 96 Non-radioactive Cytotoxicity Assay Kit, Promega, Charbonnières, France) was employed to detect subsequent LDH concentration in the media. This assay measures LDH in culture supernatants by a 30-minute coupled enzymatic assay that converts a tetrazolium salt into a red formazan product. The operations followed the manufacturer's protocol. 20 μL of lysis solution was added to positive control wells, and these cells were treated for 1h to allow complete LDH release. 75 μL of supernatant from each well was transferred to a new 96-well plate. 50 μL of cytotox 96 Reagent prepared freshly was added to each well and incubated for 30 min at room temperature without light. Sample absorbance was measured at 490 nm immediately after adding 50 μL of stop solution. The LDH release was performed and calculated as the percentage of released LDH release over the total intracellular LDH measured treated on positive

control cells. 0.1 mg/mL Triton X-100 was used as a positive control. All samples were run in triplicate.

Cell uptake

Cell uptake was measured quantitatively using flow cytometry. Raw 264.7 cells were seeded at a density of 5 X 10^4 cells/well in 12-well plates and allowed to grow overnight. C17P10 dendriplexes were prepared with fluorescent FAM-labeled siRNA at an N/P ratio of 5, as described above. These fluorescent dendriplexes were added to the medium to obtain the final fluorescent siRNA concentration of 100 nM and incubated with the cells for 2, 4, 8, and 24 h. The cells were then washed with PBS buffer three times. Cells were resuspended in PBS buffer and then analyzed by flow cytometry using an Accuri C6 (BD biosciences, Franklin Lakes, NJ, USA). Free FAM-labeled siRNA was used as a control. The relative fluorescent intensity was calculated by the ratio between the mean fluorescent intensity (MFI) of the treated samples and the negative control, after subtracting the MFI of untreated cells, following the formula below:

$$\text{Relative fluorescence intensity} = \frac{\text{MFI (dendriplexes)} - \text{MFI (cells untreated)}}{\text{MFI (free siRNA)} - \text{MFI (cells untreated)}}$$

Confocal microscopy was also used to visualize dendriplex uptake. Cells were seeded at a density of 5 × 10^4 cells/well in chambered coverslips, µ-Slide 8 well (Ibidi, Planegg, Germany). These cells were incubated for 4 and 24 h with either free fluorescent siRNA or fluorescent dendriplexes (N/P ratio of 5) at the FAM-labeled siRNA concentration of 100 nM. Before observation, the coverslips were washed with PBS and fixed using 4% (v/v) paraformaldehyde. The visualization was performed at a 63X magnification with a Zeiss LSM 510 (Carl Zeiss, Jena, Germany) fluorescence microscope equipped with a 1 mW helium−neon laser and a plan-apochromat 63X objective lens (numerical aperture 1.40, oil immersion). Differential interferential contrast (DIC) images were captured simultaneously. The pinhole was set at 1.0 Airy unit (0.8 μm optical slice thickness). The images were subsequently analyzed with LSM 510 software version 3.2 (Carl Zeiss).

in vitro inhibition of TNF-α production

Raw 264.7 cells were seeded in a 96-well plate at 8,000 cells/well density and allowed to grow overnight. The medium was then replaced with a serum-free medium containing different concentrations of C17P10 dendriplexes. These treatments were replaced with full-medium 4 h later. After 21h incubation, LPS was added at the final 10 ng/mL concentration to activate the macrophages and stimulate TNF-α production and secretion. After three additional hours of incubation, the supernatant was harvested and transferred to new 96-well plates. The concentration of secreted TNF-α was finally measured with a mouse TNF-α ELISA kit (Thermo Fisher, Villebon-Sur-Yvette, France). All samples were run in triplicate. C17P10 dendriplexes prepared with a negative control siRNA (C17P10 dendriplexes ctrl) were used to assess the sequence specificity.

Collagen-induced arthritis in mice

In vivo experimental procedures using DBA/1OlaHsd mice were approved by the ethical committee No 026 and the French ministry of education and research (Accepted protocol No 2842-2015110914248481_v5). Male DBA/1OlaHsd mice, 6-8 weeks old, 15-22g, were purchased from Envigo (Gannat, France) and let for one week after the reception for adaptation before starting the experiments. The mice were housed with access to water and food *ad libitum* and maintained at a constant temperature (19-22°C) and relative humidity (45-65%).

The collagen-induced arthritis model was performed as follows. In brief, complete Freund's adjuvant and chicken type II collagen dissolved in diluted acetic acid were mixed at a 1:1 ratio (v:v). This mixture was emulsified into a creamy emulsion using a tissue homogenizer. On day 0, after anesthesia with isoflurane, mice were injected with 50 µL of the emulsion at the tail base intradermally. A second injection (boost) was performed on day 21. After the second injection, mice were monitored every 2 days, including weight, hind paw volume, and arthritis scoring. The scoring criteria are described below.

0 = normal, 1 = one or two digits inflamed (red and thickened), 2 = all of the digits inflamed (red and thickened) and moderate swelling of the foot, 3 = redness and

increased swelling of ankle and foot, 4 = severe swelling of whole paw and digits. The hind paw volume was measured using a plethysmometer (Harvard Apparatus).

On day 25, most mice showed apparent symptoms of arthritis. Mice were assigned to 4 groups to equalize the sum of the scores of each group. On day 27, the mice were injected into the iliac plexus vein under isoflurane anesthesia with either 200 µL of PBS, 200 µL of C17P10 dendriplexes at 10 µM siRNA, 200 µL of free dendron at the equivalent concentration used for dendriplexes, or 200µL of C17P10 dendriplexes-ctrl at 10 µM siRNA. Injections were repeated on days 29, 31, and 33.

Mice were sacrificed on day 36. After sacrifice, the hind legs of CIA mice were removed immediately, fixed for 24 h in 4% paraformaldehyde, and decalcified for 8 h in Microdec (Microm Microtech, France). After decalcification, hind legs were included in paraffin blocks and sectioned in 4 µm thick slides. The specimens were stained with hematoxylin and eosin (H&E).

Synovial cell infiltration and pannus formation were individually scored by two observers in a blinded manner, using a 0–4 scale as follows [27,28]: The score for every histopathologic feature was summed for each animal: 0 = no inflammation; 1 = slight thickening of the synovial cell layer and/or some inflammatory cells in the sublining; 2 = thickening of the synovial lining and moderate infiltration of the sublining; 3 = thickening of the synovial lining and marked infiltration; 4 = thickening of the synovial lining and severe infiltration.

Statistical analysis

Results were reported as the mean ± standard error of the mean (SEM). In all experiments, statistical analysis was conducted using ANOVA and supported by the GraphPad Prism 6.0 software. *A* p-value ≤0.05 (two-tail) was considered significant.

RESULTS AND DISCUSSION

The goal of the present work was to design an amphiphilic dendron for nucleic acid delivery. A dendron with a C17 aliphatic chain and 10 pyrrolidinium surface groups (C17P10) was readily synthesized with a high yield reaching 71% (Figure 1). The pyrrolidinium surface groups were chosen as they were previously shown to be very

efficient in dendrimers to complex siRNA and to display low cytotoxicity[21]. The CMC was determined to be 0.16mM (Figure 2A). Compared to values from standard cationic surfactants such as CTAB, which possesses an aliphatic chain of 16 carbons (CMC of 1mM)[29], this CMC value is significantly lower, likely due to the dendritic structure of C17P10, which favors accessible self-assembling properties. Other amphiphilic dendrons displaying 12 charges and a slightly longer hydrophobic alkyl chain showed CMC slightly lower than the one from C17P10 dendron[30]. Due to a low CMC and the necessary structuration into micelle to complex siRNA, small dendrons could be considered for *in vivo* administration, limiting their eventual toxicity.

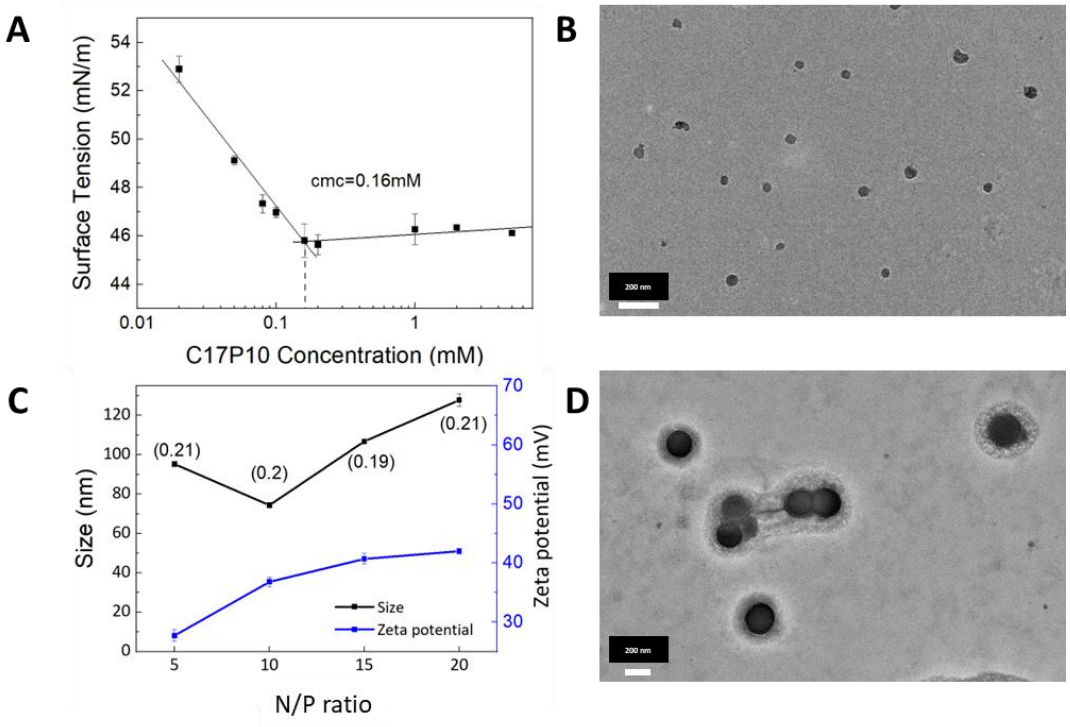

Figure 2. A: C17P10 concentration-dependent surface tension allowing CMC determination. **B:** TEM image of C17P10 micelles (osmium tetroxide staining). The scale bar represents 200 nm. **C:** Size and zeta potential of dendriplexes at the different N/P ratios. C17P10 dendriplexes PdI is indicated on the graph between brackets. **D:** Transmission electron microscope (TEM) image of C17P10 siRNA dendriplexes stained by osmium tetroxide (scale bars=200 nm).

Micelles produced from C17P10 dendrons were further characterized as such without the presence of siRNA. Their diameter, measured by DLS, was 8 ± 2 nm with a large polydispersity (PdI=0.37) and high positive zeta potential of 64 ± 3 mV. This positive surface charge due to pyrrolidinium groups favors siRNA complexation. TEM images of

micelles (Figure 2B) reveal spherical objects ranging from 10 to 20 nm, slightly larger than the size measured by DLS, probably due to the staining effect of osmium tetroxide. The diameter of C17P10 in PBS measured by DLS is also on the same order of magnitude as similar amphiphilic dendrons[30]. C17P10 dendriplexes size and zeta potential were then determined as a function of the N/P ratio (Figure 2C). Dendriplex size varies from 75 nm to 125 nm for N/P ratios from 5 to 20, respectively. The minimal size was found to be for N/P=10, probably due to a more compact structure. The zeta potential increases from 28 mV to 42 mV as the N/P ratio varies from 5 to 20 as more dendrons were present within the dendriplexes as the N/P ratio increased. Lowering the N/P ratio under 5 induced colloidal instability and aggregation. For this latest reason, these dendriplexes were further rejected from our studies. Morphology of dendriplexes was evaluated by TEM. As shown on micrographs (Figure 2D), dendriplexes exhibited spherical shapes and size around 180-200 nm, significantly larger than what was measured by DLS. This discrepancy is likely due to the staining effect of osmium tetroxide, as a sort of fuzzy shell is present on the surface of particles.

The binding affinity of C17P10 dendriplexes was investigated by agarose gel electrophoresis. Images (Figure 3A) showed a clear band for the free uncomplexed siRNAs indicative of their migration, whereas no siRNA bands were observed for the C17P10 dendriplexes at all N/P ratios. These results demonstrate the excellent binding ability of siRNA to dendrons with N/P ratio in the range of 5 to 20.

As C17P10 dendriplexes are intended for intravenous delivery, a compromise between a small size to promote accumulation in the inflamed joints and a high siRNA loading for delivering a significant amount was required. Therefore, the siRNA loading efficiency of dendriplexes at the N/P ratios of 5 and 10 was assessed by fluorescence. Results demonstrate that for both N/P ratios, almost 100% siRNA was associated with dendrons (Figure S1). Since a N/P ratio of 5 corresponds to a lower quantity of dendrons, with a constant amount of siRNA and leading to a size below 100 nm, subsequent experiments were carried out using this ratio.

The ability of dendrons to protect siRNA against degradation was evaluated. The protection of the complexed siRNA against RNase degradation was evaluated by gel electrophoresis as a function of time. As shown in Figure 3B, we observed prominent

siRNA bands even for the C17P10 dendriplexes incubated with RNase for 120 minutes, proving that no significant siRNA degradation occurred. By contrast, there was no band in the free siRNA group except for the untreated control and the 5 min treatment. (Figure 3C). These results demonstrate that dendrons can effectively protect siRNA from degradation for at least 120 min, probably by preventing RNases from accessing siRNA due to the compact structure of the dendriplexes.

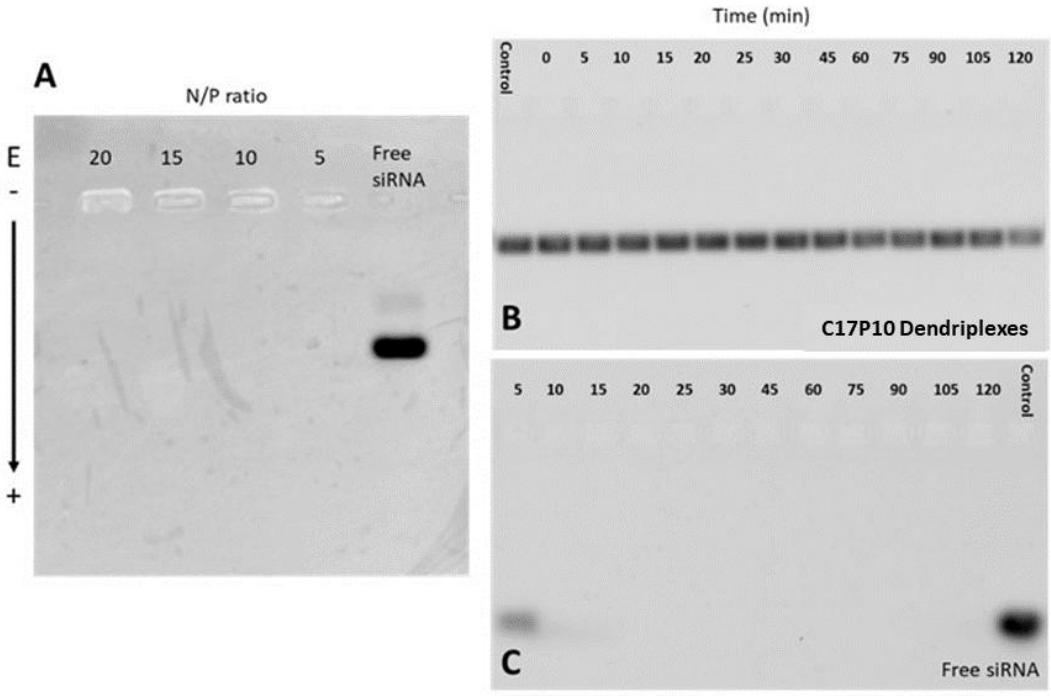

Figure 3. A) Gel electrophoresis of free siRNA and C17P10 dendriplexes at different N/P ratios. **B)** Stability against RNase over time of free siRNA and **C)** siRNA-associated C17P10 dendriplexes (time expressed in minutes).

MTT and LDH assays were performed to investigate potential cell toxicity induced by C17P10 dendrons and C17P10 dendriplexes. Experiments were carried out with C17P10 dendriplexes as a function of siRNA concentration and dendrons at their equivalent concentration in dendriplexes. As shown in Figure 4A, dendriplexes can be considered safe up to a concentration of 120nM siRNA (eq to a C17P10 dendron concentration of 3.12 µM). In contrast, at higher concentrations, both C17P10 dendrons and C17P10 dendriplexes displayed a dose-dependent decrease in viability. The cytotoxicity of

C17P10 dendriplexes is comparable to what has been observed for other cationic dendrimers with similar surface groups[21].

Interestingly, C17P10 dendriplexes show lower toxicity at an equivalent dose than C17P10 dendrons. This is most likely due to the complexation of siRNA in C17P10 dendriplexes which reduces the overall positive surface charge and holds the dendrons together, preventing them from solubilizing the cell membrane, therefore reducing the toxicity. In addition to the MTT assay, the LDH release study (Figure 4B) shows a similar pattern. C17P10 dendriplexes revealed a LDH release above 20% (percentage considered toxic) for concentrations in siRNA higher than 120 nM (corresponding to a C17P10 dendron concentration of 3.12 µM) while for free dendrons, this threshold occurs for a lower equivalent siRNA concentration of 60 nM, confirming that membrane insertion of monomeric dendrons occurs a lot less when complexed with siRNA. As both MTT and LDH assays showed that C17P10 dendriplexes were safe, up to a siRNA concentration of 120 nM (eq to a dendron concentration of 3.12 µM), further cell experiments were then carried out at this subtoxic maximum concentration.

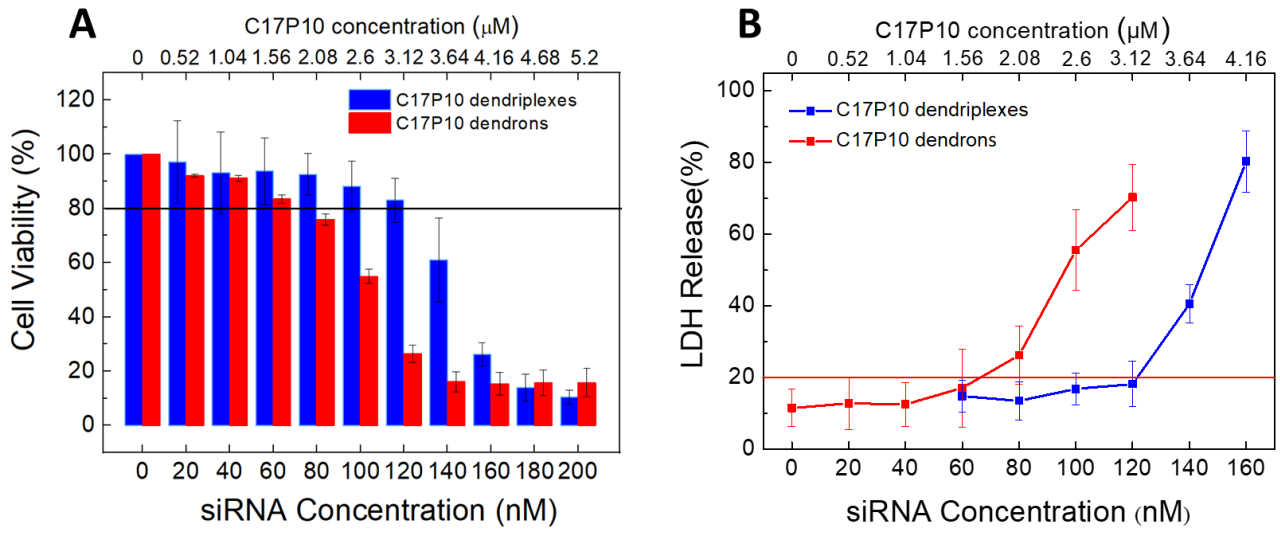

Figure 4. Cell toxicity of C17P10 dendriplexes and C17P10 dendrons was assesed by MTT (A) and Lactate dehydrogenase (LDH) release (B) n=3. The blue arrow

Confocal microscopy was then employed to image cell uptake of siRNA. Cells incubated with fluorescent FAM-labeled siRNA dendriplexes (Figure 5A) presented marked fluorescence compared to those treated with free fluorescent siRNA after 4 and 24 h, indicative that siRNA-loaded dendrons can penetrate cells efficiently. Flow cytometry was

subsequently used to measure dendriplexes cellular uptake as a function of incubation time (Figure 5 B). Results reveal an increase in the relative fluorescence intensity with longer incubation, which is 3.2 times higher for C17P10 dendriplexes than free siRNA as early as 4 h. After 8 and 24h of treatment, the relative fluorescence increases (Figure 5 B). All these data indicate the excellent penetration of siRNA-loaded C17P10 dendron in cells compared to free siRNA.

Subsequently, the ability of anti-TNF- α SiRNA dendriplexes to inhibit the production of TNF-α was investigated *in vitro* in an LPS model. The concentration of TNF-α released was determined using a commercial ELISA kit. After treatment with 100 nM dendriplexes, the TNF-α release of dendriplexes was only 19.3% of the positive control (LPS) (Figure 5 C). The inhibition of TNF-α release was dose-dependent, with 40% and 60 % release at 60 nM and 20 nM dendriplexes, respectively. By contrast, dendriplexes obtained with a control siRNA did not significantly inhibit TNF-α release (≈90%). In conclusion, C17P10 dendriplexes led to a dose-dependent and specific inhibition of TNF-α release *in vitro* on activated macrophages. These results are consistent with our previous data using dendrimers that demonstrated a similar concentration-dependent and sequence-specific gene silencing effect of the anti TNF-α siRNA that could reach an inhibition efficiency of ~80% at the siRNA concentration of 100 nM in the LPS-activated Raw 264.7 cells[21].

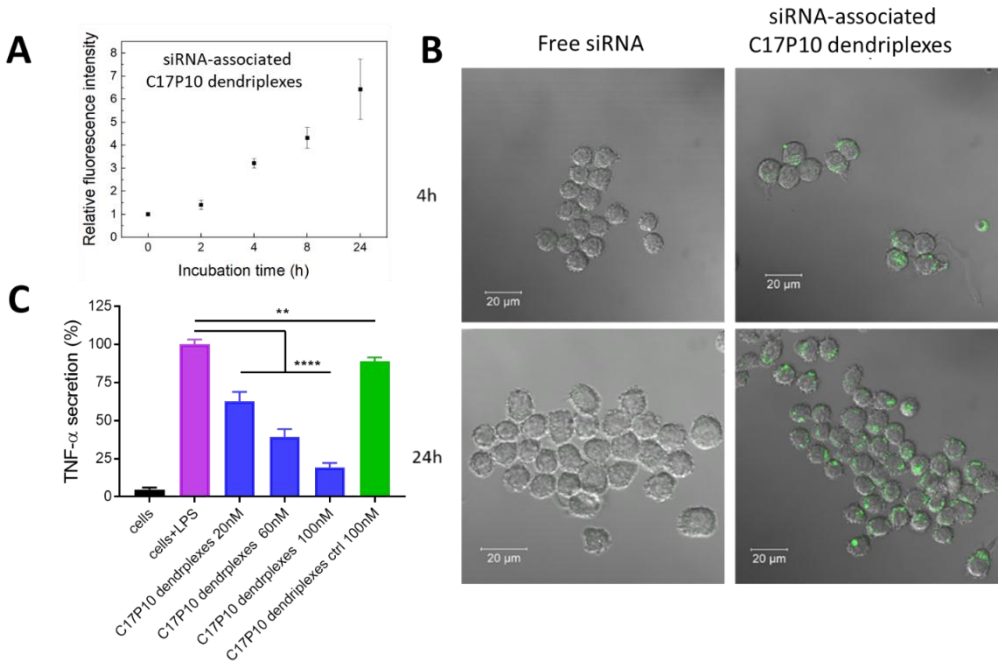

Figure 5**. A:** Cellular uptake of C17P10 siRNA complexes measured as siRNA fluorescence intensity using flow cytometry compared with free siRNA. **B:** Confocal imaging of Raw 264.7 cells incubated with siRNA-associated C17P10 dendriplexes or free siRNA for 4 h and 24 h. **C:** TNF-α secretion as a percentage of positive control (LPS) measured by ELISA on Raw 264.7 cells incubated with C17P10 dendriplexes at different concentrations or with dendriplexes with negative control siRNA. Statistical significance: ** $p < 0.01$, and *** $p < 0.001$, **** $p < 0.0001$.

Due to the potent inhibition of TNF-α induced by C17P10 dendriplexes, there were then evaluated *in vivo* in murine collagen-induced arthritis. Arthritis scoring and hind paw volume measurements were performed on the collagen-induced arthritis murine model to assess the therapeutic efficacy of dendriplexes *in vivo*. In the first *in vivo* study, only a slight change in hind paw volume was detected after three injections (Figure S2). The arthritis score did not show any significant difference between groups. The absence of effect was believed to be due to the low dose of siRNA administered (200 µL of dendriplexes at 5 µM siRNA). Based on this result, a second experiment was carried out with a 2-fold increase of the siRNA dose (200 µL of C17P10 dendriplexes at 10 µM siRNA), and a fourth injection was added. Figure 6 shows inflammation became significant a few days after the second collagen injection, on day 25. A reduction of inflammation was observed for mice treated with anti-TNF- α C17P10 dendriplexes on day 29 (after the second injection), both at the level of the arthritis score and the hind paw volume. By contrast, the other groups, C17P10 dendrons, and ctrl siRNA C17P10 dendriplexes did not differ in score or hind paw volume compared to PBS-treated animals. These results were even more evident on day 35, after 4 injections (Figures 6C and 6D). The comparison between the anti-TNF-α dendriplexes group and others was statistically significant in both scores ($p < 0.01$) and paw volume ($p < 0.0001$). This substantial difference indicates that anti-TNF- α dendriplexes can produce a noticeable anti-inflammatory therapeutic effect *in vivo* after 4 injections. The sequence dependence was confirmed by comparing anti-TNF- α siRNA-associated C17P10 dendriplexes and control siRNA-associated C17P10 dendriplexes. This effect was equivalent to the one observed in our previous studies using dexamethasone palmitate, as nanoprodrug[31] or entrapped into poly(lactide-co-glycolide) nanoparticles[32]. In both cases, a reduction of the arthritis score was observed after three intravenous administrations of 1mg/Kg of the prodrug delivered by the nanocarriers. Of course, the intracellular target is entirely

different for both types of drugs. However, it incited us to develop a promising nanoparticle formulation combining cationic palmitate dexamethasone and anti-TNF-α was recently designed and shown in vitro to produce a synergic result from both drugs effect that we believe in the future would allow reducing the given dose in both cases[33].
Subsequent histologic analyses of the tibiotalar and forefoot joints confirmed the above results. They revealed a significant reduction of synovial hyperplasia and infiltration in the dendriplexes group compared to the control (PBS) group (Figure 7 A-B). The potent TNF-α inhibition observed *in vitro* provides the primary explanation for such a strong efficiency. In a previous study, we demonstrated on the same murine model that nanoparticles of the same size, with long circulation time[34] could distribute with a high affinity in inflamed joints[31]. This process being related to a nonspecific extravasation process[35] described by many authors[7] would allow long-circulating siRNA dendriplexes to accumulate at the site of action and deliver their payload.

CONCLUSION

In this study, an original amphiphilic dendron with a low CMC was synthesized to allow siRNA complexation and the formation of small dendriplexes. After a series of characterizations, dendriplexes at the N/P ratio of 5 were considered a good compromise between size, good binding, and high siRNA concentration. At the N/P ratio of 5, anti-TNF-α SiRNA dendriplexes present an excellent inhibition of TNF-α *in vitro* and a significant anti-inflammatory effect in a murine collagen-induced arthritis model. Furthermore, the dose and sequence-dependent effect of dendriplexes were demonstrated both *in vitro* and *in vivo,* indicating that those new amphiphilic cationic dendrons present a very high potential for the delivery of siRNA.

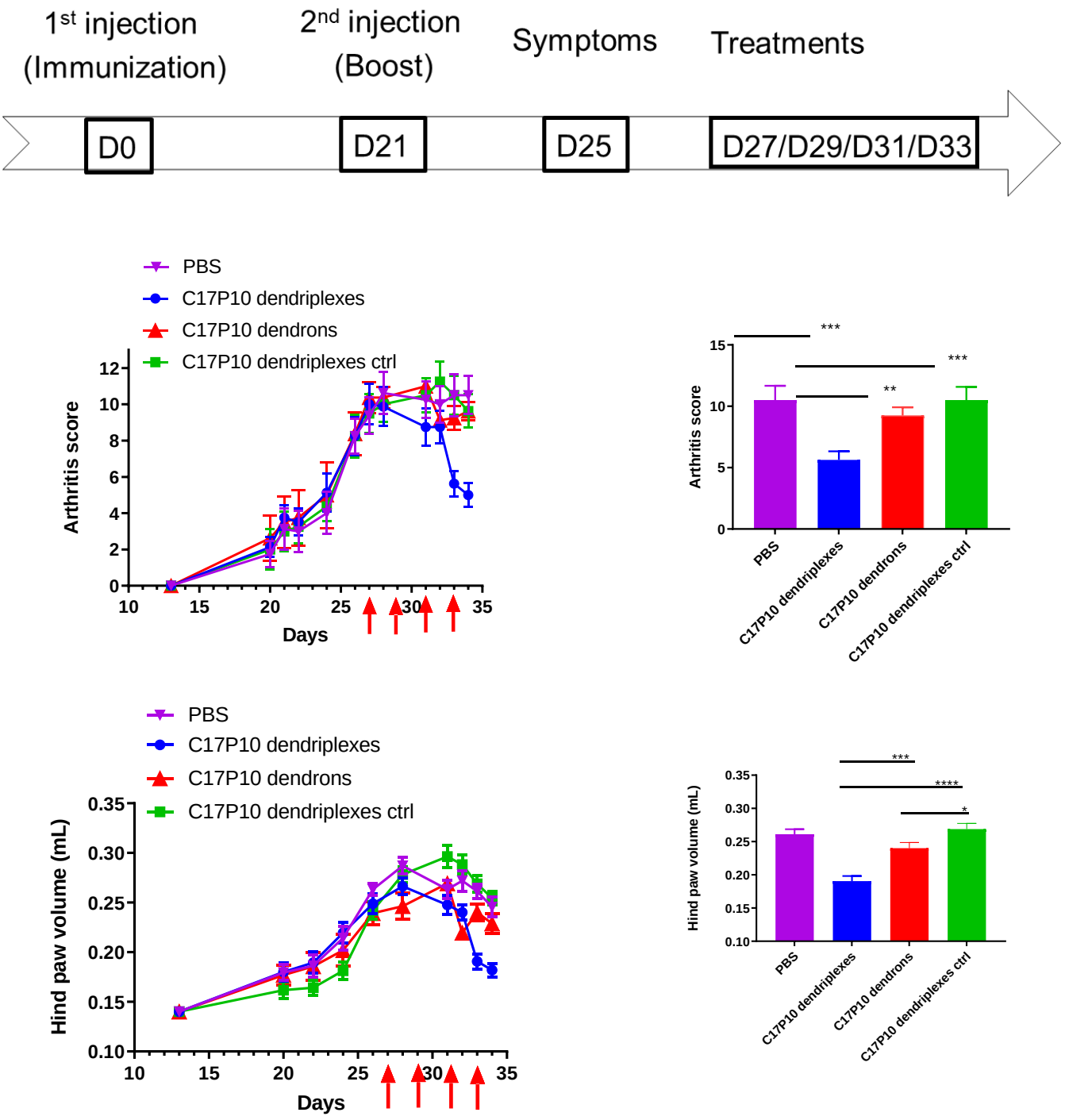

Figure 6. *In vivo efficacy* study in CIA mice model, A) Hind paw volume, B) Arthritis score and corresponding results at day 35 for Hind paw volume (C) and arthritis score (D). Statistical significance: * $p < 0.05$, ** $p < 0.01$, and *** $p < 0.001$, **** $p < 0.0001$.

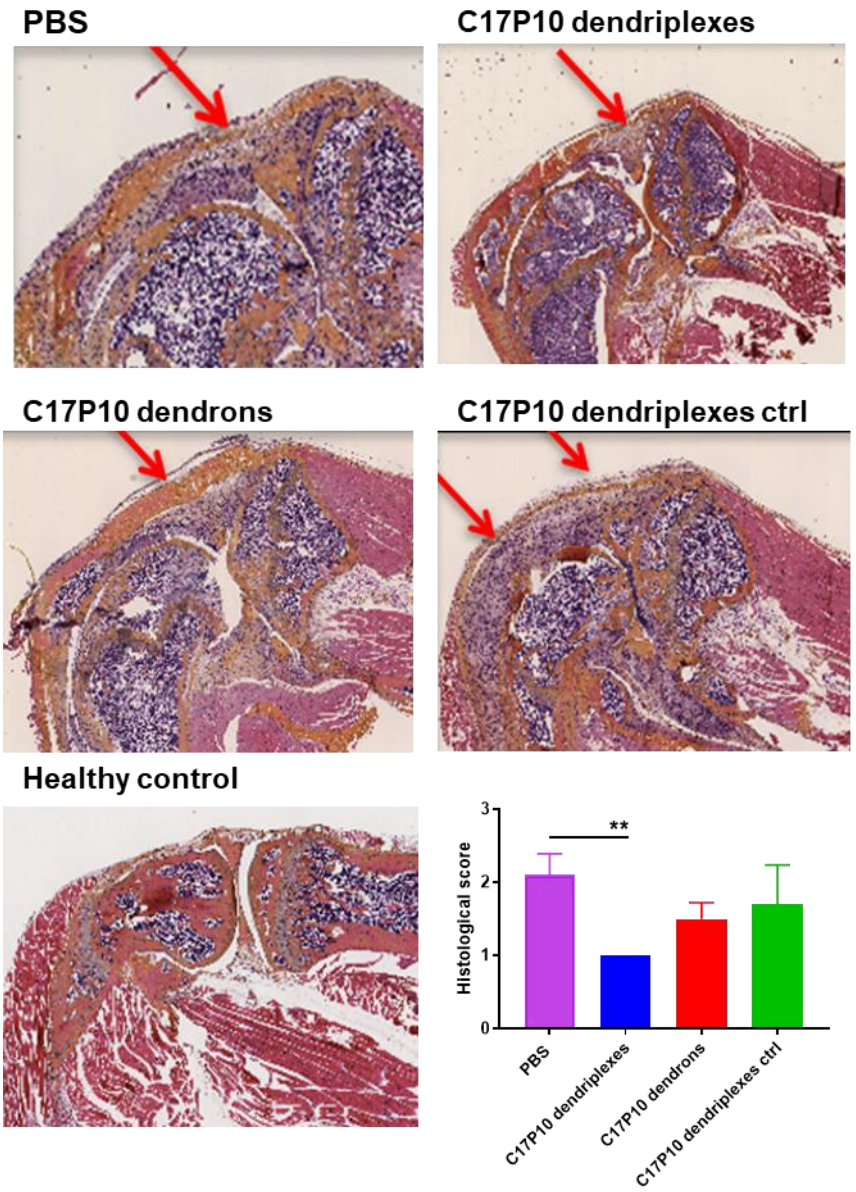

Figure 7: Histopathological evaluation of knee joint inflammation after anti-TNFα siRNA dendriplex treatment removed at day 36. a. Hematoxylin-eosin-safran (HES) staining of a representative knee for anti-TNFα siRNA dendriplex treated mice and control groups (healthy mice, PBS, dendrimers and siRNA control dendriplex). Synovial wall thickening and sublineage infiltration (arrows) were assessed in a blinded fashion and scored between 0 and 4. b. Average of the histological score for each group. n=5 knees were scored per group. Data points represent mean values ± SEM. Statistical analysis was performed with one-way ANOVA and Tuckey post-test (*p<0,05, **p<0,01)..

Acknowledgments

Zhibo Yu acknowledges financial support from China Scholarship Council. Authors would like to thank Hervé Hillaireau for fruitful discussions and Valerie Nicolas (MIPSIT,

Université Paris-Saclay) for technical assistance with confocal microscopy. Serge Mignani was granted by FCT-Fundação para a Ciência e a Tecnologia (Base Fund UIDB/00674/2020 and Programmatic Fund UIDP/00674/2020, Portuguese Government Funds) and ARDITI-Agência Regional para o Desenvolvimento da Investigação Tecnologia e Inovação through the project M1420-01-0145-FEDER-000005-CQM + (Madeira 14–20 Program). The present work has benefited from the facilities and expertise of the Electron Micoscopy facilities of Imagerie-Gif, (http://www.i2bc.paris-saclay.fr/spip.php?article282) with the precious help of C. Boulogne and C. Gillet. This core facility is a member of the Infrastructures en Biologie Santé et Agronomie (IBiSA), and is supported by the French National Research Agency under Investments for the Future programs “France-BioImaging”, and the Labex “Saclay Plant Science” (ANR-10-INSB-04-01 and ANR-11-IDEX-0003-02, respectively).

Supporting information:

siRNA loading efficiency of dendriplexes, and preliminary *in vivo* study results are presented in supporting information.

References

(1) Shuey, D. J.; McCallus, D. E.; Giordano, T. RNAi: Gene-Silencing in Therapeutic Intervention. *Drug Discov. Today* **2002**, *7* (20), 1040–1046.

(2) Jain, A.; Jain, A.; Parajuli, P.; Mishra, V.; Ghoshal, G.; Singh, B.; Shivhare, U. S.; Katare, O. P.; Kesharwani, P. Recent Advances in Galactose-Engineered Nanocarriers for the Site-Specific Delivery of SiRNA and Anticancer Drugs. *Drug Discov. Today* **2018**, *23* (5), 960–973. https://doi.org/https://doi.org/10.1016/j.drudis.2017.11.003.

(3) Hu, B.; Zhong, L.; Weng, Y.; Peng, L.; Huang, Y.; Zhao, Y.; Liang, X.-J. Therapeutic SiRNA: State of the Art. *Signal Transduct. Target. Ther.* **2020**, *5* (1), 101. https://doi.org/10.1038/s41392-020-0207-x.

(4) Adams, D.; Gonzalez-Duarte, A.; O’Riordan, W. D.; Yang, C. C.; Ueda, M.; Kristen, A. V.; Tournev, I.; Schmidt, H. H.; Coelho, T.; Berk, J. L.; Lin, K. P.; Vita, G.; Attarian, S.; Planté-Bordeneuve, V.; Mezei, M. M.; Campistol, J. M.; Buades, J.; Brannagan, T. H.; Kim, B. J.; Oh, J.; Parman, Y.; Sekijima, Y.; Hawkins, P. N.;

Solomon, S. D.; Polydefkis, M.; Dyck, P. J.; Gandhi, P. J.; Goyal, S.; Chen, J.; Strahs, A. L.; Nochur, S. V.; Sweetser, M. T.; Garg, P. P.; Vaishnaw, A. K.; Gollob, J. A.; Suhr, O. B. Patisiran, an RNAi Therapeutic, for Hereditary Transthyretin Amyloidosis. *N. Engl. J. Med.* **2018**. https://doi.org/10.1056/NEJMoa1716153.

(5) Akinc, A.; Goldberg, M.; Qin, J.; Dorkin, J. R.; Gamba-Vitalo, C.; Maier, M.; Jayaprakash, K. N.; Jayaraman, M.; Rajeev, K. G.; Manoharan, M.; Koteliansky, V.; Röhl, I.; Leshchiner, E. S.; Langer, R.; Anderson, D. G. Development of Lipidoid-SiRNA Formulations for Systemic Delivery to the Liver. *Mol. Ther.* **2009**, *17* (5), 872–879. https://doi.org/10.1038/mt.2009.36.

(6) Fattal, E.; Fay, F. Nanomedicine-Based Delivery Strategies for Nucleic Acid Gene Inhibitors in Inflammatory Diseases. *Adv. Drug Deliv. Rev.* **2021**, *175*, 113809. https://doi.org/https://doi.org/10.1016/j.addr.2021.05.019.

(7) Yu, Z.; Reynaud, F.; Lorscheider, M.; Tsapis, N.; Fattal, E. Nanomedicines for the Delivery of Glucocorticoids and Nucleic Acids as Potential Alternatives in the Treatment of Rheumatoid Arthritis. *WIREs Nanomedicine and Nanobiotechnology* **2020**, *12* (5), e1630. https://doi.org/https://doi.org/10.1002/wnan.1630.

(8) Tobon, G. J.; Youinou, P.; Saraux, A. The Environment, Geo-Epidemiology, and Autoimmune Disease: Rheumatoid Arthritis. *Autoimmun Rev* **2010**, *9* (5), A288-92. https://doi.org/10.1016/j.autrev.2009.11.019.

(9) Smolen, J. S.; Aletaha, D.; McInnes, I. B. Rheumatoid Arthritis. *Lancet* **2016**, *388* (10055), 2023–2038. https://doi.org/10.1016/S0140-6736(16)30173-8.

(10) Kim, J. W.; Suh, C. H. Systemic Manifestations and Complications in Patients with Rheumatoid Arthritis. *J. Clin. Med.* **2020**, *9* (6), 1–5. https://doi.org/10.3390/JCM9062008.

(11) Siebert, S.; Tsoukas, A.; Robertson, J.; McInnes, I. Cytokines as Therapeutic Targets in Rheumatoid Arthritis and Other Inflammatory Diseases. *Pharmacol. Rev.* **2015**, *67* (2), 280–309.

(12) Farrugia, M.; Baron, B. The Role of TNF-α in Rheumatoid Arthritis: A Focus on Regulatory T Cells. *J. Clin. Transl. Res.* **2016**, *2* (3), 84–90.

(13) Zhang, H.; Shi, N.; Diao, Z.; Chen, Y.; Zhang, Y. Therapeutic Potential of TNFα Inhibitors in Chronic Inflammatory Disorders: Past and Future. *Genes Dis.* **2021**, *8*

(1), 38–47. https://doi.org/https://doi.org/10.1016/j.gendis.2020.02.004.

(14) Li, J.; Zhang, Z.; Wu, X.; Zhou, J.; Meng, D.; Zhu, P. Risk of Adverse Events After Anti-TNF Treatment for Inflammatory Rheumatological Disease. A Meta-Analysis. *Frontiers in Pharmacology*. 2021. https://doi.org/10.3389/fphar.2021.746396.

(15) Toussirot, É.; Aubin, F. Paradoxical Reactions under TNF-α Blocking Agents and Other Biological Agents given for Chronic Immune-Mediated Diseases: An Analytical and Comprehensive Overview. *RMD Open* **2016**, *2* (2), e000239. https://doi.org/10.1136/rmdopen-2015-000239.

(16) Wang, D.; Goldring, S. R. The Bone, the Joints and the Balm of Gilead. *Mol. Pharm.* **2011**, *8* (4), 991–993. https://doi.org/10.1021/mp200328t.

(17) Yuan, F.; Quan, L. dong; Cui, L.; Goldring, S. R.; Wang, D. Development of Macromolecular Prodrug for Rheumatoid Arthritis. *Adv. Drug Deliv. Rev.* **2012**, *64* (12), 1205–1219. https://doi.org/10.1016/j.addr.2012.03.006.

(18) Pereira, P.; Barreira, M.; Queiroz, J. A.; Veiga, F.; Sousa, F.; Figueiras, A. Smart Micelleplexes as a New Therapeutic Approach for RNA Delivery. *Expert Opin. Drug Deliv.* **2017**, *14* (3), 353–371. https://doi.org/10.1080/17425247.2016.1214567.

(19) Navarro, G.; Pan, J.; Torchilin, V. P. Micelle-like Nanoparticles as Carriers for DNA and SiRNA. *Mol. Pharm.* **2015**, *12* (2), 301–313. https://doi.org/10.1021/mp5007213.

(20) Roques, C.; Fattal, E.; Fromes, Y. Comparison of Toxicity and Transfection Efficiency of Amphiphilic Block Copolymers and Polycationic Polymers in Striated Muscles. *J. Gene Med.* **2009**, *11* (3), 240–249. https://doi.org/10.1002/jgm.1304.

(21) Bohr, A.; Tsapis, N.; Andreana, I.; Chamarat, A.; Foged, C.; Delomenie, C.; Noiray, M.; El Brahmi, N.; Majoral, J. P.; Mignani, S.; Fattal, E. Anti-Inflammatory Effect of Anti-TNF-α SiRNA Cationic Phosphorus Dendrimer Nanocomplexes Administered Intranasally in a Murine Acute Lung Injury Model. *Biomacromolecules* **2017**, *18* (8), 2379–2388. https://doi.org/10.1021/acs.biomac.7b00572.

(22) Bohr, A.; Tsapis, N.; Foged, C.; Andreana, I.; Yang, M.; Fattal, E. Treatment of Acute Lung Inflammation by Pulmonary Delivery of Anti-TNF-α SiRNA with PAMAM Dendrimers in a Murine Model. *Eur. J. Pharm. Biopharm.* **2020**, *156*,

114–120. https://doi.org/10.1016/j.ejpb.2020.08.009.

(23) Chen, J.; Zhu, D.; Liu, X.; Peng, L. Amphiphilic Dendrimer Vectors for RNA Delivery: State-of-the-Art and Future Perspective. *Accounts of Materials Research*. 2022, pp 484–497. https://doi.org/10.1021/accountsmr.1c00272.

(24) Launay, N.; Caminade, A.; Lahana, R.; Majoral, J. A General Synthetic Strategy for Neutral Phosphorus-containing Dendrimers. *Angew. Chemie Int. Ed. English* **1994**, *33* (15-16), 1589–1592.

(25) Mitjaville, J.; Caminade, A.-M.; Mathieu, R.; Majoral, J.-P. New Synthetic Strategies for Phosphorus-Containing Cryptands and the First Phosphorus Spherand Type Compound. *J. Am. Chem. Soc.* **1994**, *116* (11), 5007–5008. https://doi.org/10.1021/ja00090a064.

(26) Blais, J.-C.; Turrin, C.-O.; Caminade, A.-M.; Majoral, J.-P. MALDI TOF Mass Spectrometry for the Characterization of Phosphorus-Containing Dendrimers. Scope and Limitations. *Anal. Chem.* **2000**, *72* (20), 5097–5105. https://doi.org/10.1021/ac0003854.

(27) Quan, L.; Zhang, Y.; Crielaard, B. J.; Dusad, A.; Lele, S. M.; Rijcken, C. J. F.; Metselaar, J. M.; Kostková, H.; Etrych, T. T.; Ulbrich, K.; Kostkova, H.; Etrych, T. T.; Ulbrich, K.; Kiessling, F.; Mikuls, T. R.; Hennink, W. E.; Storm, G.; Lammers, T.; Wang, D.; Kostková, H.; Etrych, T. T.; Ulbrich, K.; Kiessling, F.; Mikuls, T. R.; Hennink, W. E.; Storm, G.; Lammers, T.; Wang, D. Nanomedicines for Inflammatory Arthritis: Head-to-Head Comparison of Glucocorticoid-Containing Polymers, Micelles, and Liposomes. *ACS Nano* **2014**, *8* (1), 458–466. https://doi.org/10.1021/nn4048205.

(28) Anderson, R.; Franch, A.; Castell, M.; Perez-Cano, F. J.; Bräuer, R.; Pohlers, D.; Gajda, M.; Siskos, A. P.; Katsila, T.; Tamvakopoulos, C.; Rauchhaus, U.; Panzner, S.; Kinne, R. W. Liposomal Encapsulation Enhances and Prolongs the Anti-Inflammatory Effects of Water-Soluble Dexamethasone Phosphate in Experimental Adjuvant Arthritis. *Arthritis Res. Ther.* **2010**, *12* (4), R147. https://doi.org/10.1186/ar3089.

(29) Yu, L.; Lu, T.; Luan, Y.-X.; Liu, J.; Xu, G.-Y. Studies on the Effects of Amino Acids on Micellization of CTAB via Surface Tension Measurements. *Colloids Surfaces A*

Physicochem. Eng. Asp. **2005**, *257–258*, 375–379. https://doi.org/https://doi.org/10.1016/j.colsurfa.2004.10.066.

(30) Philippe, G.; Jingjie, T.; Ling, D.; Ahlem, B.; Aura, T.; Erik, L.; Yuanyu, H.; Zhenbin, L.; Mengjie, Z.; Samantha, F.; Laure, B.; Wenjun, L.; Eric, M.; Domenico, M.; Yuhua, W.; Xiaoxuan, L.; Suzanne, G.; Juan, I.; Sabrina, P.; Benjamin, G.; Ling, P. Self-Assembling Supramolecular Dendrimer Nanosystem for PET Imaging of Tumors. *Proc. Natl. Acad. Sci.* **2018**, *115* (45), 11454–11459. https://doi.org/10.1073/pnas.1812938115.

(31) Lorscheider, M.; Tsapis, N.; ur-Rehman, M.; Gaudin, F.; Stolfa, I.; Abreu, S.; Mura, S.; Chaminade, P.; Espeli, M.; Fattal, E. Dexamethasone Palmitate Nanoparticles: An Efficient Treatment for Rheumatoid Arthritis. *J. Control. Release* **2019**, *296*. https://doi.org/10.1016/j.jconrel.2019.01.015.

(32) Simón-Vázquez, R.; Tsapis, N.; Lorscheider, M.; Rodríguez, A.; Calleja, P.; Mousnier, L.; de Miguel Villegas, E.; González-Fernández, Á.; Fattal, E. Improving Dexamethasone Drug Loading and Efficacy in Treating Arthritis through a Lipophilic Prodrug Entrapped into PLGA-PEG Nanoparticles. *Drug Deliv. Transl. Res.* **2022**, *12* (5), 1270–1284. https://doi.org/10.1007/S13346-021-01112-3/FIGURES/8.

(33) Gürcan, S.; Tsapis, N.; Reynaud, F.; Denis, S.; Vergnaud, J.; Özer, Ö.; Fattal, E. Combining Dexamethasone and TNF-α SiRNA within the Same Nanoparticles to Enhance Anti-Inflammatory Effect. *Int. J. Pharm.* **2021**, *598*. https://doi.org/10.1016/J.IJPHARM.2021.120381.

(34) Lorscheider, M.; Tsapis, N.; Simón-Vázquez, R.; Guiblin, N.; Ghermani, N.; Reynaud, F.; Canioni, R.; Abreu, S.; Chaminade, P.; Fattal, E. Nanoscale Lipophilic Prodrugs of Dexamethasone with Enhanced Pharmacokinetics. *Mol. Pharm.* **2019**, *16* (7), 2999–3010. https://doi.org/10.1021/acs.molpharmaceut.9b00237.

(35) Deriu, M. A.; Tsapis, N.; Noiray, M.; Grasso, G.; El Brahmi, N.; Mignani, S.; Majoral, J.-P.; Fattal, E.; Danani, A. Elucidating the Role of Surface Chemistry on Cationic Phosphorus Dendrimer–SiRNA Complexation. *Nanoscale* **2018**, *10* (23), 10952–10962.